Investigation of the effect of calcination time on the antibacterial, antifungal and anticancer activities of TiO_2/ZnO nanocomposites

Adil Kadum Shakir[1], Ebrahim Ghanbari-Adivi[1], Aref S. Baron[2,3], Morteza Soltani[1]

[1]Faculty of Physics, University of Isfahan, Isfahan 8174673441, Iran

[2] Department of physics, College of science, University of Kufa, Al-Najaf, Iraq.

[3] Department of Sonar, College of Medical and Health Technologier, University of Alkafeel, Al-Najaf, Iraq.

Abstract

Nanomaterials have significantly transformed multiple scientific and technological fields due to their exceptional properties, which result from their quantum confinement effects and high surface-to-volume ratios. Among these materials, zinc oxide (ZnO) and titanium dioxide (TiO_2) nanoparticles have attracted considerable interest because of their diverse applications.

In this study, TiO_2-ZnO nanocomposites were synthesized using varying calcination times of 1, 1.5, 2, 2.5, and 3 hours. Characterization of fabricated samples through X-ray diffraction (XRD) spectroscopy, Fourier transform infrared (FTIR) spectroscopy, field emission scanning electron microscopy (FESEM), and energy-dispersive X-ray spectroscopy (EDXS) confirmed the successful fabrication of the nanocomposites. In this regard, XRD analysis revealed anatase TiO_2 and hexagonal wurtzite ZnO phases. Raman spectroscopy also supported these findings, identifying characteristic peaks of both TiO_2 and ZnO.

The calcination time had a minimal effect on the crystal structures and also morphology of the nanocomposites, which gave rise to its negligible impact on optical properties and biological activities of the samples. Optical properties assessed by means of UV-visible and photoluminescence (PL) spectroscopy showed consistent band gap absorption and emission profiles across all samples, among which the nanocomposite calcined for 1 hour exhibited the best optical properties. The sample prepared at 1 hour not only showed the most favorable optical properties, but also demonstrated significant antibacterial, antifungal, and cytotoxic activities, which make it suitable for various applications. In this regard, a reduction of more than 99.9% occurred in the number of Escherichia coli and Staphylococcus aureus bacteria and

[DOI: 10.22068/ijmse.3778]

also Candida albicans fungus by using TiO_2-ZnO nanocomposite. Besides, addition of 500 µg/ml of nanocomposite decreased the cell viability to 34.47%, which signifies its high cytotoxicity activity.

Keywords: TiO_2-ZnO nanocomposite, Calcination time, Zinc oxide, Titanium dioxide, Antibacterial activities

Introduction

Recent advances in nanotechnology have facilitated the investigation of particles whose sizes vary from 1 to 1000 nanometers. The small dimensions of these particles, compared to their larger counterparts, have resulted in their unique properties, which make them appealing for numerous applications in various sectors, including electronics, renewable energy, environmental remediation, and biomedical research [1,2]. Lots of studies have demonstrated that nanomaterials possess enhanced mechanical, electrical, magnetic, thermal, catalytic, and antimicrobial properties compared to their counterparts with larger scale. Beyond their applications in nanomedicine, nanomaterials are also influential in other fields such as nanoelectronics, biomaterials, energy production, and consumer products. Furthermore, nanotechnology holds the promise of developing a variety of novel materials and devices [3].

Thanks to their some characteristics for instance high ability in decomposition of organic and inorganic pollutants originating from photocatalytic properties and also extraordinary antimicrobial and antifungal activities, Zinc oxide (ZnO) and titanium dioxide (TiO_2) have been employed in a range of applications, consisting of biomedical, , fabrication of electrodes for water splitting, hydrogen generation, carbon dioxide reduction, solar energy conversion, drug delivery systems, sensors, and energy storage solutions. Some strategies such as doping and creation of nanocomposites have been used to enhance the antifungal effectiveness of these nanoparticles [4-6]. These materials typically act as n-type semiconductor photocatalysts, effectively breaking down a wide array of organic contaminants present in both air and wastewater. The band gap and excitation binding energies for ZnO and TiO_2 are relatively high, which are approximately 3.3 eV and 60 meV for ZnO, and 3.1 eV and 53 meV for TiO_2, respectively. The energy required for photon-induced electron excitation allowing the

[DOI: 10.22068/ijmse.3778]

transition of electrons from the valence band (VB) to conduction band (CB) primarily occurs within the ultraviolet (UV) spectrum [4].

Among many semiconductor nanomaterials, TiO_2 and ZnO have gained significant attention because of their excellent chemical stability, low toxicity, affordability, and strong antimicrobial properties [6]. The antibacterial and antifungal characteristics of metal oxide nanoparticles have been extensively investigated. The findings obtained from the conducted research indicate that ZnO demonstrates antibacterial effects and can boost the generation of reactive oxygen species (ROS) as its particle size decreases. Its antifungal properties arise from the generation of free radicals on the nanoparticles' surfaces, which do damage to the lipids in fungal cell membranes subsequently resulting in protein leakage through disrupted membranes [5,6].

TiO_2 nanoparticles exhibit antimicrobial effects even at minimal concentrations through a photocatalytic mechanism that inflicts severe damage to the targeted microorganisms. Both anatase and rutile phases of TiO_2 nanoparticles are known for their excellent antifungal properties. The widespread usage of titanium dioxide is attributed to its exceptional thermal and chemical stability along with its high photocatalytic performance. The toxicity associated with titanium dioxide nanoparticles stems from their physical characteristics rather than their chemical composition. These nanoparticles are capable of crossing biological barriers, potentially causing harm to cells or organs. Various methods have been employed to enhance the antimicrobial efficacy of titanium dioxide nanoparticles against simple microorganisms such as bacteria and viruses [5].

To overcome the challenges posed by wide band gaps and low photoenergy conversion efficiency, researchers have investigated the hybridization of noble metals with semiconducting oxides like ZnO and TiO_2. This strategy seeks to enhance the photocatalytic activity of the nanoparticles by integrating their energy levels at the heterojunction [7,8]. Therefore, in recent years, the development of hybrid nanomaterials has attracted considerable attention within the nanotechnology sector. These innovative materials have the ability to modify the properties of individual particles while introducing new and improved functionalities. However, certain nanostructures such as ZnO are often characterized by limited optical properties and also having point defects, which can restrict their direct application in different industries [9,10]. A particularly promising area of research is the creation of nanohybrid ZnO/TiO_2 materials, which merge the beneficial properties of both components.

[DOI: 10.22068/ijmse.3778]

These nanohybrids have demonstrated significant potential in applications related to antibacterial, antifungal, and anticancer activities, particularly in the context of treating skin cancer [11,12].

Recent research has showed that the synergetic effects of ZnO and TiO_2 nanoparticles can lead to improved antimicrobial effectiveness against multidrug-resistant bacteria as well as better biocompatibility [13-15]. Therefore, as mentioned above, the combination of ZnO and TiO_2 appears to be one of the most straightforward methods to enhance the antibacterial and antifungal properties of these metal oxides. Although numerous studies have investigated the antibacterial and antifungal effects of each ZnO and TiO_2, the specific antibacterial and antifungal performance of TiO_2-ZnO hybrid nanomaterials has not been thoroughly explored in the literature [16]. In a study, Najibi Ilkhechi et al. [5] synthesized ZnO, TiO_2, and ZnO–TiO_2 composite (1:1 weight ratio) using the sol-gel method. All the prepared nanoparticles inhibited the fungi growth at the concentration of 50 μg/ml, among which the TiO_2-ZnO composite exhibited superior antifungal activities compared to TiO_2 and ZnO. At 300 μg/ml, both TiO_2 and TiO_2-ZnO composite completely inhibited spur production. The morphology of the particles varied where pure ZnO was pyramidal, TiO_2 showed spherical-shaped structure, and the TiO_2-ZnO composite exhibited a combination of both of the aforementioned shapes along with additional surface growth. Notably, TiO_2-ZnO composite at lower concentrations (150 μg/ml) can increase ROS production and also result in greater oxidative stress compared to pure TiO_2 or ZnO, enhancing its antifungal activities .

In another reseach, Gunasekaran et al. [3] synthesized pure ZnO and ZnO-doped TiO_2 nanocomposites via sol-gel method to be used for degradation of methylene blue (MB) under visible light. ZnO-doped TiO_2 composite achieved an 84% degradation rate over 6 hours. Kinetic analysis showed that the degradation process follows pseudo-first-order kinetics. Additionally, the ZnO-doped TiO_2 nanocomposites exhibited enhanced antibacterial activities, which could effectively inhibited both Gram-positive and Gram-negative bacteria, including Escherichia coli and Bacillus sublittus. Also, Siwinska-Stefańska et al. [17] delineated the creation of a multifunctional TiO_2−ZnO composite through a hydrothermal approach, which exhibited strong photocatalytic capabilities. The influence of two critical parameters, including reaction time and the molar ratio of TiO_2 to ZnO, was investigated in this study on the physicochemical and structural attributes of the binary system during the hydrothermal synthesis. Their findings indicated that improvement in various properties, consisting of

[DOI: 10.22068/ijmse.3778]

morphology, crystallinity, porosity, and chemical surface characteristics, can contribute to an enhancement in photocatalytic and antibacterial activities .

This study aims at focusing on the synthesis of nanohybrid ZnO/TiO_2 materials and assess their optical properties and also antibacterial and antifungal activities.

Experimental Procedure

To fabricate ZnO nanoparticles, 8.76 gr of zinc acetate ($Zn(CH_3CO_2)_2$) and 3.19 gr of sodium hydroxide (NaOH) were separately dissolved in 20 mL of water, followed by incessant stirring at 35 °C for 20 minutes. Next, the prepared solutions were mixed and stirred for 2 hours until the formation of a milky solution. Afterward, the resulting solution was undergone to another 100minute stirring until the conversion of the solution into a gel-like substance.

In a separate stage and to synthesis TiO_2, 15 mL of titanium tetraisopropoxide (TTIP) was dissolved in 50 mL of ethanol and continuously stirred for 30 minutes. Then, 20 mL of deionized water was added into resulting solution and stirred until the formation of a white solution.

Finally and for fabrication of nanohybrid TiO_2-ZnO, the white solution obtained in the previous stage was mixed with the gel-like substance prepared in the first step and left at room temperature for 240 minutes. Afterward, the resulting mixture was centrifuged eight times (each centrifuge took 10 minutes and was performed at 10,000 rpm). Then, the product was dried in an oven at 150 °C for 10 hours. The dried product was placed in a furnace and calcinated at 700 °C for five durations of 1, 1.5, 2, 2.5, and 3 hours.

Results and Discussion

The X-ray diffraction (XRD) images of the TiO_2-ZnO nanocomposites calcinated at 700 °C and various times of 1, 1.5, 2, 2.5, and 3 hours are illustrated in Figure 1. XRD is an advantageous and powerful means to study materials from crystallographic aspect. All the XRD images were collected in the 2θ ranging from 5 to 75 degrees. According to the XRD image of the nanocomposite composed of ZnO and TiO_2 and calcinated at 1 h (Figure 1a), the peaks located at approximately 25.3, 36, 49, 53.5, 54.3, 63.4, 68.9, and 70.9 degrees can be ascribed separately to the (101), (004), (200), (105), (211), (204), (116), and (220) planes of anatase TiO_2. In addition, other peaks, including 32.8, 35.4, and 56.7 degrees respectively related to the (100), (101), and (110) planes of hexagonal wurtzite ZnO phase can be seen [18-

[DOI: 10.22068/ijmse.3778]

22]. The XRD peaks detected for the TiO_2 as well as ZnO verify the successful synthesis of the nanocomposite.

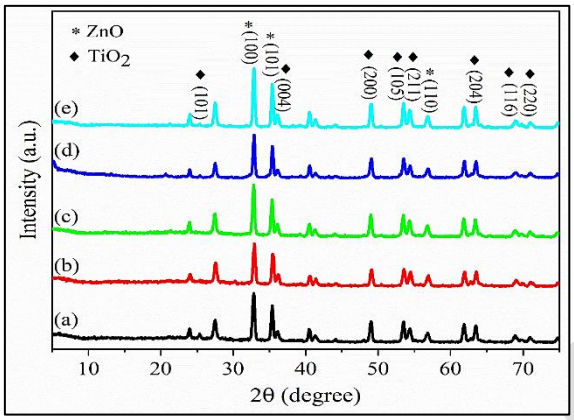

Figure 1. The XRD images of the TiO_2-ZnO nanocomposites calcinated at (a) 1, (b) 1.5, (c) 2, (d) 2.5, and (e) 3 hour(s).

As evidenced from the XRD image of the nanocomposite obtained at 1.5 h, the increment in the calcination time had negligible impact on the crystal structure of the nanocomposite (Figure 1b). Based on this fact, the peaks related to the TiO_2 and also ZnO observed for the sample obtained at 1 h are also detected for the one calcinated at the time of 1.5 h. Raising the calcination time from 1.5 to 2 h has resulted in attenuation of the intensity of (101) peak at 25.3 degrees (Figure 1c). However, the major peaks related to TiO_2 and also zinc oxide can be easily observed.

Like the nanocomposites calcinated at the times of 1 and 1.5 h, the one obtained at the time of 2.5 h shows the main peaks of TiO_2 and ZnO (Figure 1d). Accordingly, the planes related to the TiO_2 and also zinc oxide found in the XRD pattern of the nanocomposite calcinated at 1 h can be easily detected for the sample calcinated at 2.5 h. Increasing the calcination time from 2.5 to 3 h had also no considerable impact on the structure of the nanocomposite. In accordance with the XRD image of the nanocomposite synthesized at 3 h (Figure 1e), the increment in the calcination time did not change the positions of the XRD peaks and also their intensities. Besides, the planes relevant to the TiO_2 and also the ZnO can obviously be detected. As a conclusion, the calcination time insignificantly altered the structure of the nanocomposites and all the prepared samples disclosed similar XRD patterns.

Fourier transform infrared spectroscopy (FTIR) was adopted to scrutinize the functional groups such as vibrational inorganic metallic modes present within the TiO_2-ZnO nanocomposites. Figure 2 exhibits the FTIR spectra of the nanocomposites fabricated at varied calcination times.

[DOI: 10.22068/ijmse.3778]

Referring to the FTIR spectrum of the nanocomposite obtained at calcination time of 1 h (Figure 2a), the peak found at the wavenumber of 3430 cm^{-1} is typically ascribed to the absorption band of hydroxyl (O–H) of H_2O molecules within the nanocomposite.

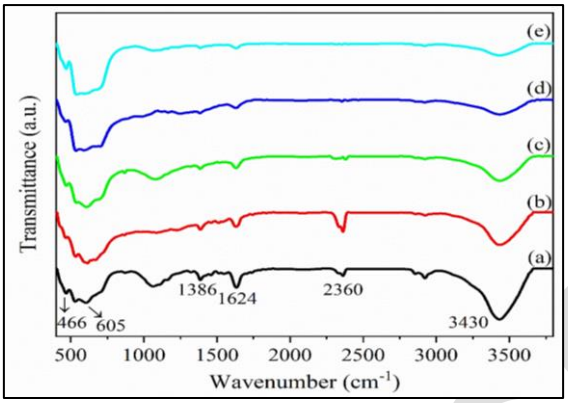

Figure 2. The FTIR spectra of the TiO_2-ZnO nanocomposites synthesized at the times of (a) 1, (b) 1.5, (c) 2, (d) 2.5, and (e) 3 hour(s).

The absorption band detected at approximately 2360 cm^{-1} corresponds to the C-O bending of physisorbed carbon dioxide (CO_2) molecules present in the air [23]. The peaks observed at the wavenumbers of 1624 and 1386 cm^{-1} can respectively attributed to the remaining sp^2 carbon and tertiary C–OH groups. According to references, the stretching modes of inorganic metallic bond are usually detected in the range from 400 to 800 cm^{-1} [24]. As a result, the broad characteristic peak situated at about 605 cm^{-1} is pertinent to the stretching vibrations of Ti–O bonds [25]. Moreover, the pronounced peak seen at the wavenumber of 466 cm^{-1} is relevant to the Zn-O bond [26-28]. The peaks found in the FTIR spectrum of the TiO_2-ZnO nanocomposite calcinated at 1 h corroborate the successful synthesis of the nanocomposite.

Raising the calcination time from 1 to 1.5 h has led to no effect on the FTIR spectrum of the TiO_2-ZnO nanocomposite (Figure 2b). Accordingly, the absorption band of O-H bond in H_2O molecules, the peak corresponding the physisorbed CO_2 molecules, and the absorption bands assigned to the residual sp^2 carbon and tertiary C–OH groups can easily be detected. Moreover, the characteristic peaks pertinent to the Ti–O and Zn-O bonds can be observed.

Figure 2c illustrates the FTIR spectrum of the TiO_2-ZnO nanocomposite prepared at the time of 2 h, which is taken in the range approximately from 500 to 3750 cm^{-1}. Obviously, the peak pertinent to the O-H bond in H_2O molecules is observed. Moreover, the peak demonstrating physisorbed CO_2 molecules, the peak showing the residual sp^2 carbon, and the peak related to the tertiary C–OH groups can be seen. The peaks of Ti–O and Zn-O bonds are detectable for

[DOI: 10.22068/ijmse.3778]

the TiO_2-ZnO nanocomposite calcinated at the time of 2 h, implying the successful fabrication of the sample.

The increment in the calcination times of the TiO_2-ZnO nanocomposites from 2 to 2.5 h and also from 2.5 to 3 h has inconsiderably influenced the FTIR spectra of the samples (Figures 2d, e). Analogous to other TiO_2-ZnO nanocomposites, the well-defined peaks of Ti–O bonds found at 605 cm^{-1} and the peak of Zn-O observed at 466 cm^{-1} can also be seen for the nanocomposites synthesized at the times of 2.5 and 3 h. As the FTIR spectra of the nanocomposites disclosed, increasing the calcination time had negligible effect on their spectra. And, similar FTIR spectra were shown by all the samples.

Field emission scanning electron microscopy (FE-SEM) was chosen to morphologically investigate the prepared TiO_2-ZnO nanocomposites and the FESEM images recorded from the surface of the samples are demonstrated in Figure 3. As evidenced by the FESEM image of the TiO_2-ZnO nanocomposite calcinated at the time of 1 h (Figure 3a), the spherical-shaped titanium dioxide particles and the rod-type zinc oxide nanoparticles are apparently visible [18]. The size of the round-shaped TiO_2 particles exceeds 1 µm. However, the ZnO particles possess a nanometer scale. By raising the calcination time to 1.5 h, no obvious change is observed in the morphology of the TiO_2-ZnO nanocomposite (Figure 3b). Accordingly, the rod-shaped ZnO nanoparticles are also detected for the TiO_2-ZnO nanocomposite prepared at the time of 1.5 h. The round-shaped TiO_2 particles buried under the rod-shaped ZnO nanoparticles. No change was detected in the size of the titanium dioxide and zinc oxide particles with increasing the calcination time.

[DOI: 10.22068/ijmse.3778]

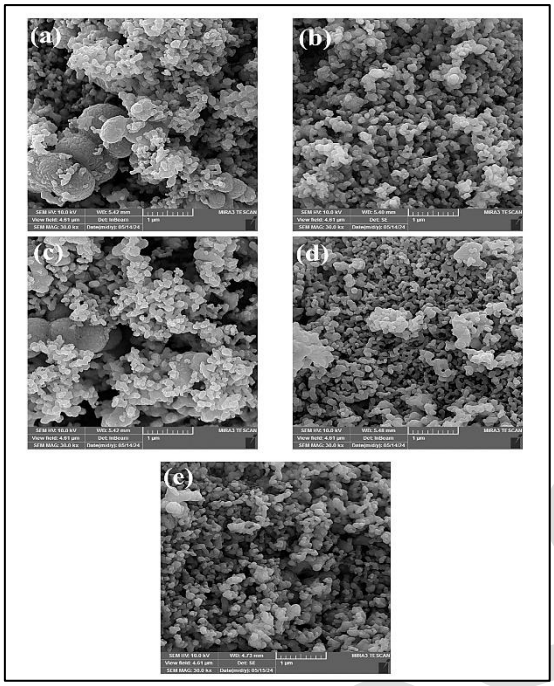

Figure 3. The FESEM images taken from the TiO_2-ZnO nanocomposites calcinated at the times of (a) 1, (b) 1.5, (c) 2, (d) 2.5, and (e) 3 hour(s).

Like other samples, in the FESEM image of the TiO_2-ZnO nanocomposite prepared at the time of 2 h, the TiO_2 particles with a round shape and the ZnO nanoparticles having the rod shape are discovered (Figure 3c). With increasing the calcination time, no visible change can be found in the diameter of both titanium dioxide and zinc oxide particles.

The rise in the time of the calcination process from 2 to 2.5 h has resulted in appearance of some agglomerated particles. Based on Figure 3d, the ZnO particles having the shape of rod are detected for the TiO_2-ZnO nanocomposite obtained at the time of 2.5 h; however, some agglomerated ZnO particles can be found in this sample, which were not observed in the TiO_2-ZnO nanocomposites calcinated at the times of 1, 1.5, and 2 hours. Analogous to the sample synthesized at the time of 2.5 h, the one fabricated at the time of 3 h manifests the agglomerated ZnO particles (Figure 3e), meaning that the increasing the calcination time to the 2.5 and also 3 h can cause production of agglomerated ZnO particles, which can negatively affect the optical and also antibacterial performance of the TiO_2-ZnO nanocomposite.

Figure 4 demonstrates the energy dispersive X-ray spectroscopy (EDXS) patterns of the nanocomposites synthesized at varied times, consisting of 1, 1.5, 2, 2.5, and 3 hours. The EDXS is a beneficial technique to investigate the chemical composition of the materials.

[DOI: 10.22068/ijmse.3778]

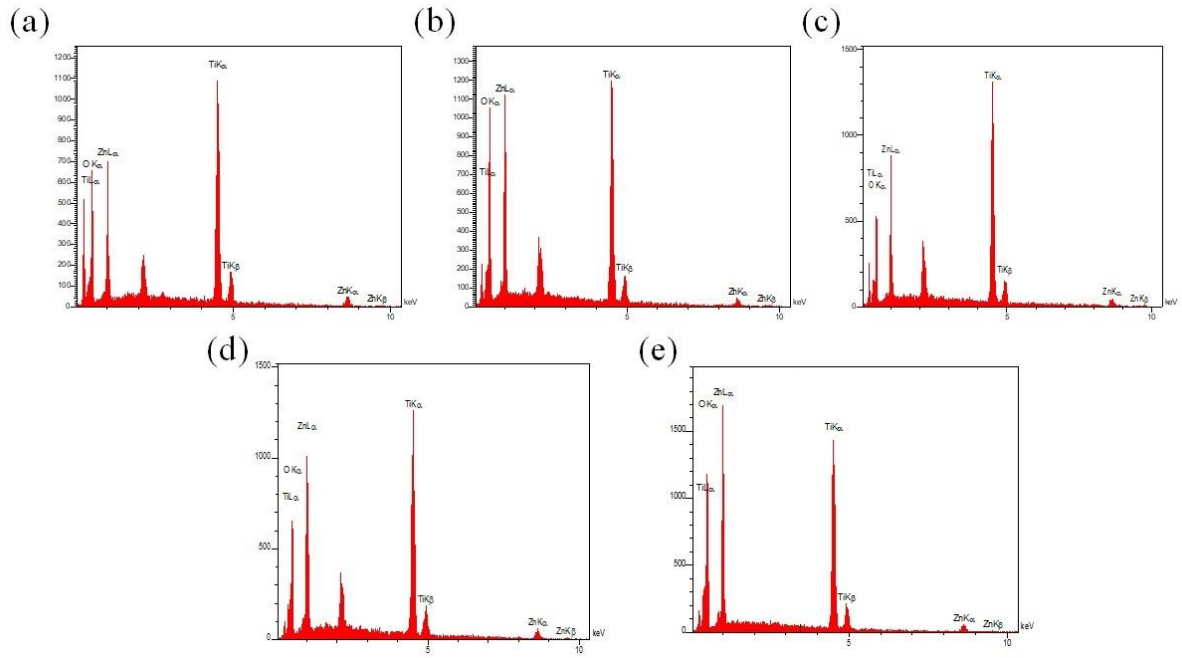

Figure 4. The EDXS pattern of the TiO_2-ZnO nanocomposites prepared at the times of (a) 1, (b) 1.5, (c) 2, (d) 2.5, and (e) 3 hour(s).

Based on the EDXS pattern of the nanocomposite calcinated at the time of 1 h (Figure 4a), the characteristic peaks of Ti element found at approximately 0.5, 4.5, and 5 keV testify the presence of the titanium-containing species within the nanocomposite. In addition to Ti element, some Zn peaks relevant to the zinc-based particles are detected, which are situated at 1, 8.5, and 9.5 keV. The peaks showing the existence of the titanium- and zinc-containing species inside the nanocomposite are also observed in the EDXS pattern of the sample constructed at the time of 1.5 hours. In this regard, the pronounced peaks of Ti and Zn elements are easily seen (Figure 4b).

Raising the calcination time from 1.5 to 2, 2.5, and 3 hours had no influence on the chemical composition of the nanocomposite (Figures 4c,d,e). The EDXS patterns of the nanocomposites calcinated at 2, 2.5, and 3 hours exhibit the major peaks of Ti and Zn elements, which attest the presence of titanium- and zinc-containing species. .

In the Raman spectrum of the nanocomposite calcinated at the time of 1 h (Figure 5a), the peaks located at about 140.7 and 609.8 cm^{-1} can separately be imputed to the vibrations of E_g and B_2g of anatase TiO_2 [19,20]. The peak at ~341.9 cm^{-1} is associated with the multiple phonons scattering of zinc oxide. In addition to this peak, another peak verifying the presence of the zinc oxide nanoparticles appears at 446.6 cm^{-1}, which stems from the E_2 vibrational mode of the oxygen (O) atoms inside the zinc oxide particles. At 710.7 cm^{-1}, a peak is found which

[DOI: 10.22068/ijmse.3778]

is because of the E_1 mode of zinc oxide [19, 20]. Raising the calcination time to 1.5 h has resulted in significant change in the Ranam spectroscopy of the nanocomposite (Figure 5b). According to the Raman spectrum of the nanocomposite obtained at the time of 1.5 h, the peaks relevant to the anatase TiO_2 and wurtzite ZnO seen in Figure 5a are completely disappeared.

However, the change of the calcination time from 1.5 to 2 h led to appearance of the Raman peaks were not found for the nanocomposite calcinated at 1.5 h (Figure 5c). Accordingly, the Raman peaks at 140.7 and 609.8 cm^{-1} relevant to the vibrations of E_g and B_2g of anatase titanium dioxide are visible. Besides, the peak at 341.9 cm^{-1} assigned to the multiple phonons scattering of zinc oxide, the peak at 446.6 cm^{-1} assigned to the E_2 mode of the O atoms within the zinc oxide particles, and the peak at 710.7 cm^{-1} owing to the E_1 mode of zinc oxide can easily be detected. Like other samples, the TiO_2-ZnO nanocomposites calcinated at the times of 2.5 and 3 h reveal the peaks related to the titanium dioxide and zinc oxide (Figure 5d, e). As the characterization tests of XRD, FTIR, FESEM, EDXS, and Raman corroborated, the TiO_2-ZnO nanocomposites were successfully fabricated at different times of 1, 1.5, 2, 2.5, and 3 hours.

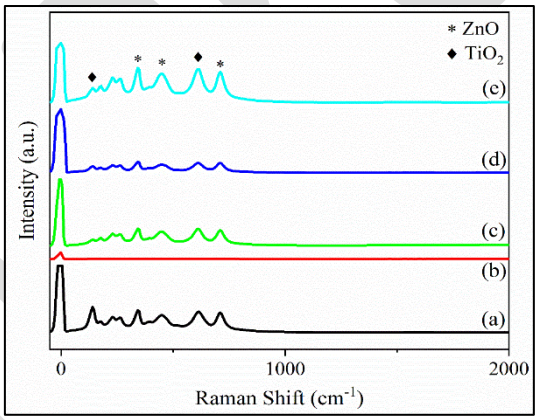

Figure 5. The Raman spectra of the nanocomposites calcinated at the times of (a) 1, (b) 1.5, (c) 2, (d) 2.5, and (e) 3 hour(s).

The optical property of the nanocomposites calcinated at 1, 1.5, 2, 2.5, and 3 h was measured using the UV-Visible spectroscopy. Figure 6a demonstrates the diffuse UV-Visible spectrum of the TiO_2-ZnO nanocomposite prepared at the calcination time of 1 hour. Accordingly, a strong and broad absorption peak is clearly observed in the wavelength ranging from 300 to 400 nm. This peak is located in the UV region and shows the band gap absorption edge [21]. The increment in the calcination time has resulted in no obvious change in the UV-Visible spectrum of the TiO_2-ZnO nanocomposites and no redshift or blueshift occurred. Referring to

[DOI: 10.22068/ijmse.3778]

the diffuse UV-Visible spectrum of the TiO_2-ZnO nanocomposite obtained at the time of 2 h (Figure 6b), the strong and broad peak seen in Figure 6a is also found for this sample. As a result, the nanocomposite possesses an optical property in the UV region, which is arisen from inter band electronic transitions.

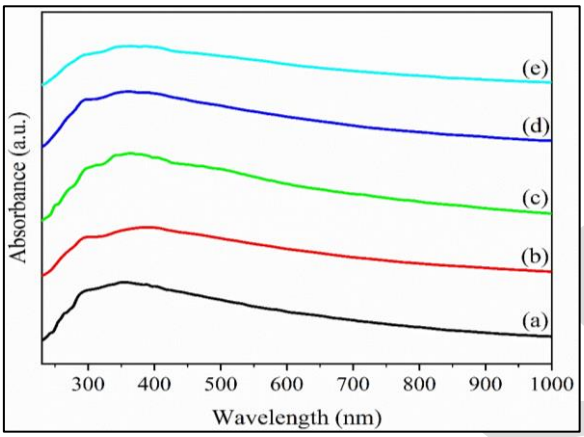

Figure 6. The UV-Visible spectra of the TiO_2-ZnO nanocomposites calcinated at the times of (a) 1, (b) 1.5, (c) 2, (d) 2.5, and (e) 3 hour(s).

Like the nanocomposites calcinated at the times of 1 and 1.5 h, the one prepared at 2 h also exhibits the strong and broad absorption peak in the wavelength ranging from 300 to 400 nm (Figure 6c). No change can be detected in the position of the absorption peak with the increasing of the calcination time. In other words, no redshift or blueshift is observed with the increment in the calcination time. The peak in the range from 300 to 400 nm is situated in the UV region, which originates from the inner band electronic transitions.

In the spectrum of the nanocomposite fabricated at 2.5 hours, the broad peak situated in the UV region can be found (Figure 6d). This peak, like other samples, is located in the range from 300 to 400 nm, which is evidence for possessing of the nanocomposite from an optical property in the UV region. Figure 6e exhibits the diffuse UV-Visible spectrum of the TiO_2-ZnO nanocomposite calcinated at the time of 3 h. As we saw for the aforementioned samples, this nanocomposite also manifests the absorption peak in the UV region, which is in the wavenumber ranging from 300 to 400 nm. As a consequence, all the TiO_2-ZnO nanocomposites calcinated at different times take the advantage of optical property, which is in the UV region. In addition, with increasing the calcination time, no noticeable change was observed in the position of the absorption peak.

Figure 7 illustrates the photoluminescence (PL) images of the nanocomposites calcinated at the times of 1, 1.5, 2, 2.5, and 3 h. Two emission peaks can commonly be found in the metal oxide

[DOI: 10.22068/ijmse.3778]

materials, one of which is observed in the UV region and related to the near band edge emissions. The other peak is usually detected in the visible region, which is arisen from the deep-level emissions. The former has strong intensity and stems from the free exciton recombination. But, the latter possesses weaker intensity and is arisen from oxygen defects. Deep-level emissions are seen in the visible region and are made from the recombination of photogenerated holes. Visible spectrum is typically composed of several individual parts, including UV-violet, violate, violet-blue, blue, and green section located roughly at 395, 423, 458, 500 and 501 nm [22-28].

Figure 7a demonstrates the PL image of the nanocomposite synthesized 1 hour. Accordingly, a sharp peak is found near the wavelength of 350 nm, which is in the UV region. In addition to this peak, another peak can be detected at the wavelength near 700 nm, which is weaker in comparison with the one seen at 350 nm. The peak at 700 nm is in the red-section of visible region and imputed to the deep-level emission. The increasing the calcination time of the TiO_2-ZnO nanocomposites from 1 to 1.5 h has led to no obvious change in the position of the PL peaks. As evidenced by PL spectrum of the nanocomposite obtained at 1.5 hours (Figure 7b), the sharp peak at 350 nm in the UV region and the peak at 700 nm in the visible region are found.

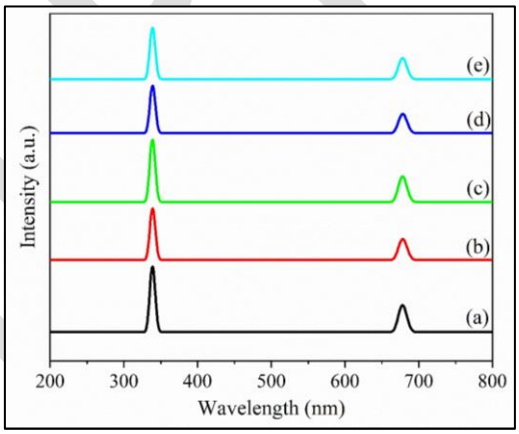

Figure 7. The PL spectra of the TiO_2-ZnO nanocomposites prepared at (a) 1, (b) 1.5, (c) 2, (d) 2.5, and (e) 3 hour(s).

Analogous to nanocomposites prepared at 1 and 1.5 h, the one calcinated at the time of 2 h shows the PL peaks at 350 and 700 nm. Accordingly, in the PL image of the nanocomposite obtained at the time of 2 h (Figure 7c), two well-defined peaks at 350 and 700 nm are detected, which are respectively in the UV and visible regions. In accordance with the Figures 7d,e showing respectively the PL images of the nanocomposites calcinated at 2.5 and 3 hours, two

[DOI: 10.22068/ijmse.3778]

pronounced peaks are visible, which are located at 350 and 700 nm. These peaks are characteristic of the near band edge and the deep-level emissions, respectively. Among all the samples, the one obtained at the time of 1 h roughly shows higher intensity in both of the PL peaks, and this sample was assigned for the study of antibacterial, antifungal, and anticancer activity.

Table 1 depicts the results obtained from the quantitative evaluation of the antibacterial and antifungal activity of the nanocomposite calcinated at 1 h against various organisms, including Escherichia coli (E. coli), Staphylococcus aureus, and Candida albicans. Their images are also demonstrated in Figure 8.

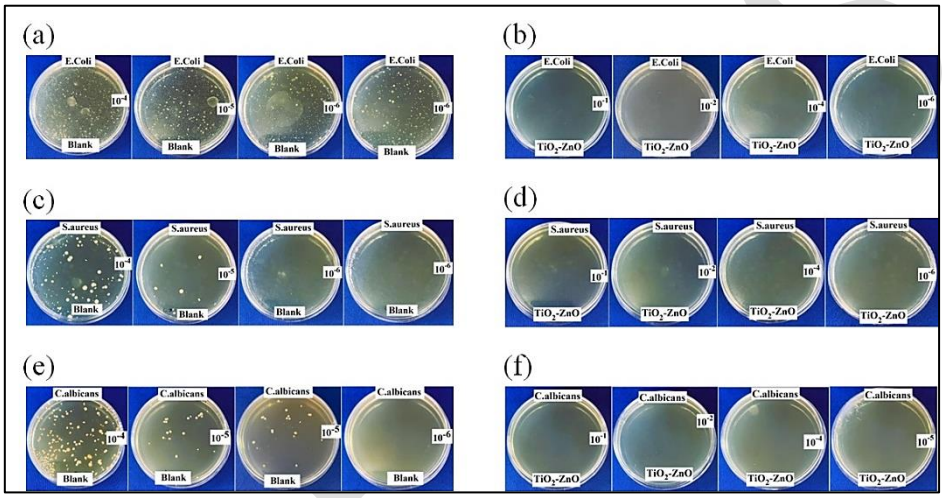

Figure 8. The antibacterial and antifungal activity of the blank sample and the nanocomposite against different microorganisms.

Colony forming unit (CFU) is a parameter to determine the number of organisms. Referring to Table 1, the number of Escherichia coli bacteria detected before the contact with both blank and TiO_2-ZnO nanocomposite samples was 1.78×10^5 ml. However, after the contact for 24 h, the results changed remarkably. Accordingly, a CFU of 3.22×10^8 ml was acquired for the blank sample, much higher than the one obtained before the contact. On the other hand, the number of Escherichia coli bacteria considerably decreased after contact with TiO_2-ZnO nanocomposite for 24 h. In this regard, the CFU exhibited by the TiO_2-ZnO nanocomposite against Escherichia coli bacteria was less than 10 ml, equals to a reduction of >99.99999%. This means that our fabricated nanocomposites are immensely effective against E. coli. Absence of the nanocomposite had no impact on the reduction of the bacteria and the blank sample had no antibacterial activity. The superb performance of TiO_2-ZnO nanocomposites in

[DOI: 10.22068/ijmse.3778]

antibacterial test can be related to their high capability in cell wall destruction, and metal-based nanoparticles typically demonstrate high activity against microorganisms [29].

Table 1. Antibacterial and antifungal properties of the nanocomposite at the time of 1 h against different microorganisms.

Microorganism	Sample	CFU (ml) at zero contact time	Sample Concentration (mg/ml)	Contact Time (h)	CFU/ml	Reduction (%)
Escherichia coli	TiO_2-ZnO	1.78×10^5	8	24	<10	>99.99999 %
	Blank		8		3.22×10^8	-
Staphylococcus Aureus	TiO_2-ZnO	3.1×10^5	8	24	<10	>99.999 %
	Blank		8		1.8×10^6	-
Candida albicans	TiO_2-ZnO	6.00×10^4	8	24	<10	>99.999 %
	Blank		8		3.25×10^6	-

In addition to Escherichia coli, Staphylococcus aureus bacteria were also chosen to examine the antibacterial activity of nanocomposites. Before exposure to samples, the CFUs recorded for both of the blank and TiO_2-ZnO nanocomposites were 3.1×10^5 ml. After 24 h contact with the blank sample, the number of Staphylococcus aureus bacteria increased and the CFU reached 1.8×10^6 ml, implying that the sample devoid of TiO_2-ZnO nanocomposite had no antibacterial activity. But, in the TiO_2-ZnO nanocomposite, a reduction of > 99.999% occurred in the number of Staphylococcus aureus bacteria and the CFU for this sample decreased from 3.1×10^5 ml to less than 10 ml. As a consequence, our proposed TiO_2-ZnO nanocomposites benefit from extraordinary antibacterial activity against different types of bacteria.

Candida albicans is a kind of fungus employed for the study of the antifungal properties of the nanocomposites. As the data listed in Table 1 clearly show, the number of Candida albicans fungi detected before the contact with 8 mg/ml blank sample and the sample with TiO_2-ZnO nanocomposite was 6.00×10^4 ml. However, after 24-hour contact with blank sample, the number of Candida albicans fungi increased remarkably, and it reached from 6.00×10^4 ml to

[DOI: 10.22068/ijmse.3778]

3.25×10^6 ml. Inclusion of TiO_2-ZnO nanocomposite into the sample led to a >99.999% reduction in the number of Candida albicans fungi. In this direction, the CFU reduced from 6.00×10^4 ml to less than 10 ml, attesting the excellent antifungal properties of our prepared nanocomposites. As the results of the effectiveness of nanocomposites against microorganisms testified, our fabricated nanocomposites are hugely effective against bacteria and fungi. Moreover, the calcination time had no effect on the activity of the nanocomposites.

In addition to the quantitative evaluation, the effectiveness of the nanocomposites calcinated at different times against various organisms, including E. coli, Staphylococcus aureus, and Candida albicans were also examined by means of disk diffusion test. Zone of inhibition of the samples against E. coli bacteria are brought in Table 2.

Table 2. Zone of inhibition of the samples against Escherichia coli bacteria.

Sample	The diameters of the inhibition zones (mm)	Number of Test	Concentration
1 h	19	1	100 µl
	19	2	
1.5 h	17	1	100 µl
	18	2	
2 h	18	1	100 µl
	16	2	
2.5 h	14	1	100 µl
	15	2	
3 h	13	1	100 µl
	15	2	
Gentamicin	28	1	30 µl
	27.5	2	
	28	3	
Distillated water	No	1	100 µl
	No	2	
	No	3	

No antibacterial activity is observed for the distillated water (blank) sample. However, the samples containing TiO_2-ZnO nanocomposites showed high effectiveness against Escherichia coli bacteria. By raising the calcination time, the zone of inhibition decreased, meaning the reduction of the effectiveness of the samples against bacteria. The best results were acquired

[DOI: 10.22068/ijmse.3778]

for the nanocomposites calcinated at the time of 1 h. According to literature, increasing the calcination time can result in agglomeration of the particles, which can subsequently diminish the antibacterial activities of the samples [30]. As the FESEM images of our fabricated samples demonstrated, some agglomerated particles appeared for the nanocomposites calcinated at 2.5 and 3 hours, which negatively affected their antibacterial activities.

The antibacterial activity of our fabricated nanocomposites were compared with gentamicin. Clearly, the activity of the sample prepared at 1 hour is comparable with gentamicin. The zone of inhibition of the samples against Staphylococcus aureus bacteria are depicted in Table 3. Like the Escherichia coli bacteria, the blank sample exhibited no antibacterial activity against Staphylococcus aureus bacteria.

Table 3. Inhibition zone of the samples against Staphylococcus aureus.

Sample	The diameters of the inhibition zones (mm)	Number of Test	Concentration
1 h	21	1	100 µl
	20	2	
1.5 h	20	1	100 µl
	20	2	
2 h	19	1	100 µl
	18	2	
2.5 h	15	1	100 µl
	16	2	
3 h	13	1	100 µl
	15	2	
Gentamicin	31	1	30 µg
	31	2	
	31	3	
Distillated water	No	1	100 µl
	No	2	
	No	3	

On the other hand, by inclusion of the TiO_2-ZnO nanocomposites into the diffusion disks, antibacterial activity is observed for the samples. All the TiO_2-ZnO nanocomposites calcinated

[DOI: 10.22068/ijmse.3778]

at the times of 1, 1.5, 2, 2.5, and 3 h revealed antibacterial activity against Staphylococcus aureus bacteria, and the best results were obtained for the one fabricated at 1 h. Interestingly, an increment in the calcination time has resulted in a reduction in the antibacterial activity. The effectiveness of the nanocomposites synthesized at 1 h is comparable with the diffusion disk containing gentamicin. The zone of inhibition of the samples against Candida albicans fungi can be found in Table 4. Accordingly, the blank sample showed no effectiveness against Candida albicans fungi. However, the samples prepared at various calcination times revealed antifungal activity, and the one obtained at the time of 1 h showed the best antifungal activity. Increasing the calcination time has led to reduction of antifungal activity. Besides, the effectiveness of the nanocomposites synthesized at the time of 1 h is comparable with the diffusion disk containing clotrimazole.

Table 4. Inhibition zone of the samples against Candida albicans.

Sample	The diameters of the inhibition zones (mm)	Number of Test	Concentration
1 h	15	1	100 µl
	16	2	
1.5 h	16	1	100 µl
	14	2	
2 h	15	1	100 µl
	13	2	
2.5 h	14	1	100 µl
	12	2	
3 h	12	1	100 µl
	10	2	
Gentamicin	20	1	50 µg
	19	2	
	20	3	
Distillated water	No	1	100 µl
	No	2	
	No	3	

The anticancer activity of the TiO_2-ZnO nanocomposites calcinated at the time of 1 h was studied by means of MTT assay whose results are shown in Table 5. In addition, the effects of various concentrations of TiO_2-ZnO nanocomposite on skin cell line are demonstrated in Figure 9. The MTT assay was carried out after 24 h incubation. According to Table 5, the

[DOI: 10.22068/ijmse.3778]

control sample (free of TiO_2-ZnO nanocomposite) shows a viability of 100%. On the other hand, introduction of 15.625 µg/ml TiO_2-ZnO nanocomposite has resulted in a decrement in the cell viability. Accordingly, the cell viability decreased from 100% to 99.55%, meaning that the TiO_2-ZnO nanocomposite can be effective against the cancer cells. The increment in the dosage of TiO_2-ZnO nanocomposites increased their cytotoxicity activity or decreased the cell viability (Figure 10). In this regard, increasing the concentration of TiO_2-ZnO nanocomposite from 15.625 to 31.25 µg/ml decreased the cell viability from 99.55% to 97.24%. Besides, for the concentrations of 62.5, 125, and 250 µg/ml, cell viabilities of 90.45, 70.26, and 45% were respectively obtained, showing that increasing the amount of the TiO_2-ZnO nanocomposite can have positive impact on their anticancer activity. The best cytotoxicity activity was exhibited by the sample with the concentration of 500 µg/ml. Accordingly, inclusion of 500 µg/ml TiO_2-ZnO nanocomposite decreased the cell viability to 34.47%. As a consequence, our TiO_2-ZnO nanocomposites prepared at the time of 1 h can be a good inhibitor for the growth of cancer cells.

Table 5. The anticancer activity of the nanocomposites prepared at 1 hour examined by MTT assay.

Concentration (µg/ml)	**Control**	**15.625**	**31.25**	**62.5**	**125**	**250**	**500**
Viability (%)	100	99.55	97.24	90.45	70.26	45	34.47

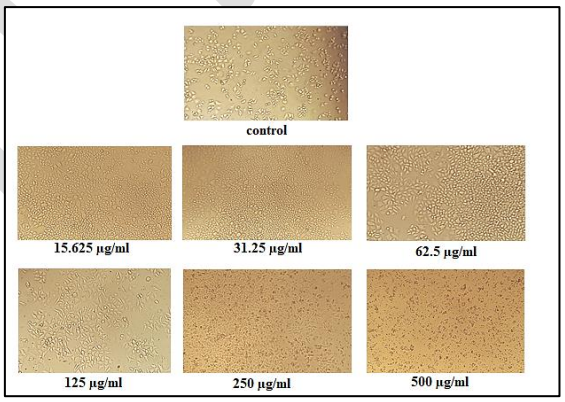

Figure 9. The effect of TiO_2-ZnO nanocomposite calcinated at the time of 1 h on skin cell line after 24 h by inverted microscope

[DOI: 10.22068/ijmse.3778]

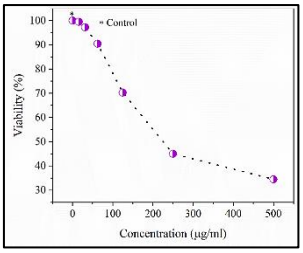

Figure 10. The relative cell viability recorded at various amounts of the nanocomposite calcinated at 1 hour.

Conclusions

In our study, TiO_2-ZnO nanocomposites with different calcination time were successfully fabricated and characterized. In this regard, five calcination times, including 1, 1.5, 2, 2.5, and 3 h were adopted. Several characterization tests, consisting of XRD, FESEM, and EDXS, were employed to investigate the influence of the calcination time on the structure and morphology of the nanocomposites.

In accordance with the XRD images of all fabricated samples, the peaks related to anatase titanium dioxide and wurtzite zinc oxide were easily found. The aforementioned peaks corroborated the fabrication of the TiO_2-ZnO nanocomposites. Calcination time influenced inconsiderably the XRD patterns of the samples and subsequently their crystallite structures. Like the XRD analysis, the FESEM test confirmed the preparation of the TiO_2-ZnO nanocomposites where the round-shaped and rod-shaped structures were respectively attributed to the TiO_2 and ZnO nanoparticles. It was deemed that the increasing the calcination time up to 2.5 hours can result in production of more agglomerated nanoparticles. The results obtained from the EDXS technique were in consistent with the XRD and FESEM analyses where the peaks pertinent to the titanium and zinc elements were evidently detected. No change was seen in the EDXS patterns of all the TiO_2-ZnO nanocomposites. Raman spectroscopy also attested the existence of TiO_2 and ZnO where the vibrations of anatase titanium dioxide and also zinc oxide particles were detected. As the characterization tests of XRD, FESEM, EDXS and Raman spectroscopy verified, all the TiO_2-ZnO nanocomposites calcinated at the various times of 1, 1.5, 2, 2.5, and 3 h were synthesized and the calcination time can have insignificant impact on the morphology and structure of the nanocomposites.

In accordance with the UV-Visible spectra of all the TiO_2-ZnO nanocomposites taken to examine their optical property, a strong and broad absorption peak was vividly detected in the wavelength ranging from 300 to 400 nm. This peak was located in the UV region and exhibited

[DOI: 10.22068/ijmse.3778]

the band gap absorption edge. Like the diffuse UV-Visible spectroscopy, all the nanocomposites manifested similar PL spectra. Accordingly, the peak at the wavelength of 700 nm in the UV region and the peak at the wavelength of 350 nm in the visible region were observed for all the nanocomposites. Also, based on PL spectroscopy, the nanocomposite prepared at the time of 1 h showed the best optical property, and was chosen for the study of antibacterial and antifungal activity. In addition, the samples obtained at the time of 1 h decreased the number of different organisms, which verified their outstanding antibacterial and antifungal activity. This sample also revealed excellent cytotoxicity activity against the cancer cells. As a result, our proposed TiO_2-ZnO nanocomposites can not only be appropriate for optical applications, but also be beneficial for their antibacterial, antifungal, and cytotoxicity activity. They can offer substantial potential for a variety of applications such as medicine, environmental science, and more. .

Reference

[1] Chaudhary, A., Kumar, N., Kumar, R., Salar, R.K., *"Antimicrobial activity of zinc oxide nanoparticles synthesized from Aloe vera peel extract". SN Applied Sciences* 2019, 1, 1-9.

[2] Raj, L., Jayalakshmy, E., *"A biogenic approach for the synthesis and characterization of zinc oxide nanoparticles produced by Tinospora cordifolia". Int J Pharm Pharm Sci* 2015, 7, 384-386.

[3] Gunasekaran, A., Rajamani, A.K., Masilamani, C., Chinnappan, I., Ramamoorthy, U., Kaviyarasu, K.J.C., *"Synthesis and characterization of ZnO doped TiO_2 nanocomposites for their potential photocatalytic and antimicrobial applications". Catalysts* 2023, 13, 215.

[4] Ghamarpoor, R., Fallah, A., Jamshidi, M.J.A.o., *"A review of synthesis methods, modifications, and mechanisms of ZnO/TiO_2-based photocatalysts for photodegradation of contaminants". ACS omega* 2024, 9, 25457-25492.

[5] Ilkhechi, N.N., Mozammel, M., Khosroushahi, A.Y.J.P.B., *"Physiology, Antifungal effects of ZnO, TiO_2 and ZnO-TiO_2 nanostructures on Aspergillus flavus". Pestic. Biochem. Physiol.* 2021, 176, 104869.

[6] Mozammel, M., Khoroushahi, A.Y., *"Antifungal effects of ZnO, TiO_2 and ZnO-TiO_2 nanocomposite on Aspergillus flavus"*. 2020.

[7] Sarathi, R., Sheeba, N., Essaki, E.S., Sundar, S.M., *"Titanium doped Zinc Oxide nanoparticles: A study of structural and optical properties for photocatalytic applications". Materials Today: Proceedings* 2022, 64, 1859-1863.

[DOI: 10.22068/ijmse.3778]

[8] Dathan, P.C., Nallaswamy, D., Rajeshkumar, S., Joseph, S., Ismail, S., Ajithan, L., Jose, L., *"A Review on Biomedical Applications of Titanium Dioxide". Trends in Biomaterials & Artificial Organs* 2023, 37, 49-54.

[9] Pragathiswaran, C., Smitha, C., Barabadi, H., Al-Ansari, M.M., Al-Humaid, L.A., Saravanan, M., *"TiO_2@ZnO nanocomposites decorated with gold nanoparticles: Synthesis, characterization and their antifungal, antibacterial, anti-inflammatory and anticancer activities". Inorganic Chemistry Communications* 2020, 121 108210.

[10] Chakra, C.S., Rajendar, V., Rao, K.V.,. Kumar, M., *"Enhanced antimicrobial and anticancer properties of ZnO and TiO_2 nanocomposites". 3 Biotech* 2017,7 1-8.

[11] Rajendran, R., Mani, A., *"Photocatalytic, antibacterial and anticancer activity of silver-doped zinc oxide nanoparticles". Journal of Saudi Chemical Society* 2020, 24 1010-1024.

[12] Ahmed, N., Tanveer, K., Younas, Z., Yousaf, T., Ikram, M., Raja, N.I., Mashwani, Z.-u.-R., Alghamdi, S., Al-Moraya, I.S., Shesha, N.T., *"Green-processed nano-biocomposite (ZnO–TiO_2): Potential candidates for biomedical applications". Green Processing and Synthesis* 2023, 12, 20230076.

[13] Nguyen, T.A., Nguyen, T.V., Nguyen-Tri, P., *"Effect of Silver Decoration and Light Irradiation on the Antibacterial Activity of TiO_2 and ZnO Nanoparticles".* 2019.

[14] Akhavan, O., *"Lasting antibacterial activities of Ag–TiO_2/Ag/a-TiO_2 nanocomposite thin film photocatalysts under solar light irradiation". Journal of colloid and interface science* 2009, 336, 117-124.

[15] Mohapatra, S., Nguyen, T.A., Nguyen-Tri, P., *"Noble metal-metal oxide hybrid nanoparticles: Fundamentals and applications".* Elsevier, 2018.

[16] Daou, I., Moukrad, N., Zegaoui, O., Rhazi Filali, F.J.W.S., *"Antimicrobial activity of ZnO-TiO_2 nanomaterials synthesized from three different precursors of ZnO: influence of ZnO/TiO_2 weight ratio". Water Sci Technol* 2018, 77, 1238–1249.

[17] Siwińska-Stefańska, K., Kubiak, A., Piasecki, A., Dobrowolska, A., Czaczyk, K., Motylenko, M., Rafaja, D., Ehrlich, H., Jesionowski, T.J.A.S.S., *"Hydrothermal synthesis of multifunctional TiO_2-ZnO oxide systems with desired antibacterial and photocatalytic properties". Appl. Surf. Sci.* 2019, 463, 791-801.

[18] Johra, F.T., Jung, W.-G.J.A.C.A.G., *"RGO–TiO_2–ZnO composites: synthesis, characterization, and application to photocatalysis". Applied Catalysis A: General* 2015, 491, 52-57.

[DOI: 10.22068/ijmse.3778]

[19] Prasannalakshmi, P., Shanmugam, N.J.M.S.i.S.P., *"Fabrication of TiO_2/ZnO nanocomposites for solar energy driven photocatalysis". Mater. Sci. Semicond. Process.* 2017, 61, 114-124.

[20] Sethi, D., Sakthivel, R., *"ZnO/TiO_2 composites for photocatalytic inactivation of Escherichia coli". Journal of Photochemistry & Photobiology, B: Biology* 2017, 168, 117-123.

[21] Wang, N., Li, X., Wang, Y., Hou, Y., Zou, X., Chen, G.J.M.L., *"Synthesis of ZnO/TiO_2 nanotube composite film by a two-step route". Materials Letters* 2008, 62,3691-3693.

[22] Das, D., Mondal, P.J.R.a., *"Low temperature grown ZnO: Ga films with predominant c-axis orientation in wurtzite structure demonstrating high conductance, transmittance and photoluminescence". RSC advances* 2016, 6, 6144-6153.

[23] Rafiq, M.Y., Iqbal, F., Aslam, F., Bilal, M., Munir, N., Sultana, I., Ashraf, F., Manzoor, F., Hassan, N., Razaq, A., *"Fabrication and characterization of ZnO/MnO_2 and ZnO/TiO_2 flexible nanocomposites for energy storage applications". J. Alloys Compd.* 2017, 729, 1072-1078.

[24] Jun, M.-C., Park, S.-U., Koh, J.-H.J.N.r.l., *"Comparative studies of Al-doped ZnO and Ga-doped ZnO transparent conducting oxide thin films". Nanoscale research letters* 2012, 7, 1-6.

[25] Mousa, H.M., Alenezi, J.F., Mohamed, I.M., Yasin, A.S., Hashem, A.F.M., Abdal-Hay, A., *Synthesis of TiO_2@ZnO heterojunction for dye photodegradation and wastewater treatment". J. Alloys Compd.* 2021, 886, 161169.

[26] Kurudirek, S.V., Kurudirek, M., Klein, B.D.B., Summers, C.J., Hertel, N.E., *"Methods in Physics Research Section A: Accelerators, Detectors, A. Equipment, Synthesis and photoluminescence properties of Ga-doped ZnO nanorods by a low temperature solution method". Nucl. Instrum. Methods Phys. Res. A* 2018, 904, 158-162.

[27] Al-Asedy, H.J., Bidin, N., Abbas, K.N., Al-Azawi, M.A., *"Structure, morphology and photoluminescence attributes of Al/Ga co-doped ZnO nanofilms: Role of annealing time". Mater. Res. Bull* 2018, 97, 71-80.

[28] Phan, D.T., Farag, A.A.M., Yakuphanoglu, F., Chung, G.S., *"Optical and photoluminescence properties of Ga doped ZnO nanostructures by sol-gel method". J. Electroceramics* 2012, 29, 12-22.

[29] Pragathiswaran, C., Smitha, C., Abbubakkar, B.M., Govindhan, P., Krishnan, N.A., *"Synthesis and characterization of TiO_2/ZnO–Ag nanocomposite for photocatalytic degradation of dyes and anti-microbial activity". Materials Today: Proceedings* 2021, 45, 3357-3364.

[DOI: 10.22068/ijmse.3778]

[30] Ismail, A.M., Menazea, A.A., Kabary, H.A., El-Sherbiny, A.E., Samy, A., *"The influence of calcination temperature on structural and antimicrobial characteristics of zinc oxide nanoparticles synthesized by Sol–Gel method". Journal of Molecular Structure* 2019, 1196, 332-337.

[DOI: 10.22068/ijmse.3778]